WASP-South hot Jupiters: WASP-178b, WASP-184b, WASP-185b & WASP-192b

Coel Hellier[1], D.R. Anderson[1,2], K. Barkaoui[3,4], Z. Benkhaldoun[3], F. Bouchy[5], A. Burdanov[6], A. Collier Cameron[7], L. Delrez[6,8], M. Gillon[6], E. Jehin[6], L.D. Nielsen[5], P.F.L. Maxted[1], F. Pepe[5], D. Pollacco[2], F.J. Pozuelos[4,6], D. Queloz[8], D. Ségransan[5], B. Smalley[1], A.H.M.J. Triaud[9], O.D. Turner[1,5], S. Udry[5], and R.G. West[2]

[1] *Astrophysics Group, Keele University, Staffordshire, ST5 5BG, UK*
[2] *Department of Physics, University of Warwick, Gibbet Hill Road, Coventry CV4 7AL, UK*
[3] *Oukaimeden Observatory, High Energy Physics and Astrophysics Laboratory, Cadi Ayyad University, Marrakech, Morocco*
[4] *Astrobiology Research Unit, Université de Liège, Liége, Belgium*
[5] *Observatoire astronomique de l'Université de Genève 51 ch. des Maillettes, 1290 Sauverny, Switzerland*
[6] *Space sciences, Technologies and Astrophysics Research (STAR) Institute, Université de Liège, Liège 1, Belgium*
[7] *SUPA, School of Physics and Astronomy, University of St. Andrews, North Haugh, Fife, KY16 9SS, UK*
[8] *Cavendish Laboratory, J J Thomson Avenue, Cambridge, CB3 0HE, UK*
[9] *School of Physics & Astronomy, University of Birmingham, Edgbaston, Birmingham, B15 2TT, UK*

date

ABSTRACT

We report on four new transiting hot Jupiters discovered by the WASP-South survey. WASP-178b transits a $V = 9.9$, A1V star with $T_{\rm eff} = 9350 \pm 150$ K, the second-hottest transit host known. It has a highly bloated radius of 1.81 ± 0.09 $R_{\rm Jup}$, in line with the known correlation between high irradiation and large size. With an estimated temperature of 2470 ± 60 K, the planet is one of the best targets for studying ultra-hot Jupiters that is visible from the Southern hemisphere. The three host stars WASP-184, WASP-185 and WASP-192 are all post-main-sequence G0 stars of ages 4–8 Gyr. The larger stellar radii (1.3–1.7 $M_\odot$) mean that the transits are relatively shallow (0.7–0.9%) even though the planets have moderately inflated radii of 1.2–1.3 $R_{\rm Jup}$. WASP-185b has an eccentric orbit ($e = 0.24$) and a relatively long orbital period of 9.4 d. A star that is 4.6 arcsec from WASP-185 and 4.4 mag fainter might be physically associated.

Key words: Planetary Systems – stars: individual (WASP-178, WASP-184, WASP-185, WASP-192)

1 INTRODUCTION

Since its start in May 2006 the WASP-South survey for transiting exoplanets operated until mid 2016, obtaining data on over 2500 nights and recording 400 billion photometric data points on 10 million stars. From 2006 to mid-2012 WASP-South used 200-mm, f/1.8 lenses, searching for transits of stars of $V = 9$–13, and obtaining typically 20 000 data points on each star. Coverage adds up to the whole sky between declination +8° and –70°, other than the crowded galactic plane, with each field being observed in typically 3 or 4 different years. In mid-2012 WASP-South switched to 85-mm, f/1.2 lenses, changing the useful magnitude range to V = 6.5–11.5, with the aim of finding the very brightest hot-Jupiter hosts such as WASP-189 (Anderson et al. 2018).

WASP-South transit candidates proved well matched to follow-up with the 1.2-m Euler telescope and CORALIE spectrograph, teamed with the TRAPPIST-South photometric telescope and (more recently) TRAPPIST-North, which together observed 1600 planet candidates. So far WASP-South has led to the announcement of 154 transiting exoplanets (34 of them jointly with data from WASP-South's northern counterpart, SuperWASP).[1]

Follow-up of WASP-South candidates is now nearing completion, and in any case such surveys are rapidly being superseded by the space-based TESS survey (Ricker et al. 2016). We report here four new transiting hot Jupiters. While WASP-184b and WASP-192b are routine hot Jupiters transiting fainter, V = 12, stars, WASP-178b transits a bright A1V star that is the hottest of the WASP planet hosts, while WASP-185b has an eccentric, 9.4-d orbit.

[1] See https://wasp-planets.net

Table 1. Observations

Facility	Date	Notes
WASP-178:		
WASP-South	2006 May–2014 Aug	101 600 points
CORALIE	2017 Apr–2018 Jul	23 RVs
EulerCAM	2018 Mar 26	I filter
WASP-184:		
WASP-South	2007 Feb–2012 Jul	24 300 points
CORALIE	2015 Jun–2018 Jul	19 RVs
TRAPPIST-South	2016 Mar 05	blue-block
EulerCAM	2018 Apr 11 02	R filter
WASP-185:		
WASP-South	2006 May–2012 Jun	34 000 points
CORALIE	2015 Jun–2018 Aug	24 RVs
TRAPPIST-South	2014 Apr 09	z band
TRAPPIST-North	2019 Jun 09	z band
WASP-192:		
WASP-South	2006 May–2012 Jul	42 200 points
CORALIE	2016 Jun–2019 Apr	12 RVs
TRAPPIST-South	2016 Apr 17	blue-block
TRAPPIST-South	2019 Jun 06	$I + z$ band

2 OBSERVATIONS

The WASP-South photometry was accumulated into multi-year lightcurves for every catalogued star, which were then searched for transits using automated routines (Pollacco et al. 2006; Collier Cameron et al. 2007b), followed by human vetting of the search outputs. Planet candidates were then listed for followup observations by the TRAPPIST-South 0.6-m robotic photometer (e.g. Gillon et al. 2013) and the Euler/CORALIE spectrograph (e.g. Triaud et al. 2013). Transit photometry for the stars reported here was also obtained with the EulerCAM photometer (e.g. Lendl et al. 2012) and with TRAPPIST-North (Barkaoui et al. 2019). Our observations are listed in Table 1.

For three of our stars (WASP-184, WASP-185 and WASP-192) the CORALIE spectra were reduced to radial-velocity measurements using a standard G2 mask (Pepe et al. 2002), while for the hotter star WASP-178 we used an A0 mask. The resulting values are listed in Table A1.

As we routinely do for WASP-South planet discoveries, we used the WASP photometry, typically spanning 6 months of observation in a year and several years of coverage, to look for rotational modulations of the planet-host stars. Our methods are detailed in Maxted et al. (2011). For the four stars reported here we found no significant modulations with upper limits of 1–2 mmags (as reported in the Tables for each star).

3 SPECTRAL ANALYSES

We combined the CORALIE spectra for each object in order to make a spectral analysis. For three of the stars discussed here (WASP-184, WASP-185 and WASP-192) we adopt the same methods used in recent WASP-South papers (e.g. Hellier et al. 2019a), as described by Doyle et al. (2013). Thus we estimated the effective temperature, $T_{\rm eff}$, from the Hα line, and the surface gravity, $\log g$, from Na I D and Mg I b lines. We also translate the $T_{\rm eff}$ value to give an indicative spectral type. To estimate the metallicity, [Fe/H], we make equivalent-width measurements of unblended Fe I lines, quoting errors that take account of the uncertainties in $T_{\rm eff}$ and $\log g$. We use the same Fe I lines to measure $v \sin i$ values, taking into account the CORALIE instrumental resolution ($R = 55\,000$) and adopting macroturbulence values from Doyle et al. (2014). The spectral analysis values are reported in the Tables for each star.

WASP-178 is much hotter than the above stars, with $T_{\rm eff} = 9350 \pm 150$ K. For this star we measured over 100 clean, unblended, Fe I and Fe II lines in the spectral range 500–600 nm. The stellar parameters of $T_{\rm eff}$, $\log g$ and microturbulence were obtained by iteratively adjusting them, using non-linear least squares, in order to find the values which minimized the scatter in the abundance obtained from the Fe lines. This procedure simultaneously attempts to remove any trends in abundance with excitation potential (temperature diagnostic) and equivalent width (microturbulence diagnostic), as well as any differences between the Fe I and Fe II lines (surface gravity diagnostic). The parameter uncertainties were obtained from the residual scatter in the optimal solution (see Niemczura et al. 2014 for further discussion on stellar parameter determination).

4 SYSTEM PARAMETERS

Our process for parametrising the systems combines all our data, photometry and radial-velocity measurements, in one Markov-chain Monte-Carlo (MCMC) analysis, using a code developed in several iterations from that originally described by Collier Cameron et al. (2007a).

Our standard procedure (see, e.g., Hellier et al. 2019a) places a Gaussian "prior" on the stellar mass. We derive this using the stellar effective temperature and metallicity, from the spectral analysis, and an estimate of the stellar density, from initial analysis of the transit. These are used as inputs to the BAGEMASS code (Maxted et al. 2015), based on the GARSTEC stellar evolution code (Weiss & Schlattl 2008), which then outputs estimates for the stellar mass and age. WASP-178 is too hot for the BAGEMASS code to be reliable, so we instead adopted a mass prior of 2.04 ± 0.12 M$_\odot$, from expectations of a main-sequence star of its temperature (e.g. Boyajian et al. 2013), followed by checking that this models the transit to give a self-consistent set of parameters.

In more recent WASP-South papers, following the availability of GAIA DR2 parallaxes (Gaia Collaboration et al. 2016, 2018), we also place a prior on the stellar radius. We apply the Stassun & Torres (2018) correction to the parallax to produce a distance estimate, and then use the Infra-Red Flux Method (Blackwell & Shallis 1977) to arrive at the stellar radius. Before the GAIA DR2, getting the stellar radius wrong was one of the commonest sources of systematic error in transit analyses, and thus a prior on the radius improves the reliability of the solution and can make up for limitations in the transit photometry (see, e.g., Hellier et al. 2019b).

In modelling the RVs we first allowed an eccentric orbit (which is required for WASP-185) but where it was not required (the other three systems) we enforced a circular orbit (as discussed in Anderson et al. 2012, this makes use of the expectation that the time for tidal circularisa-

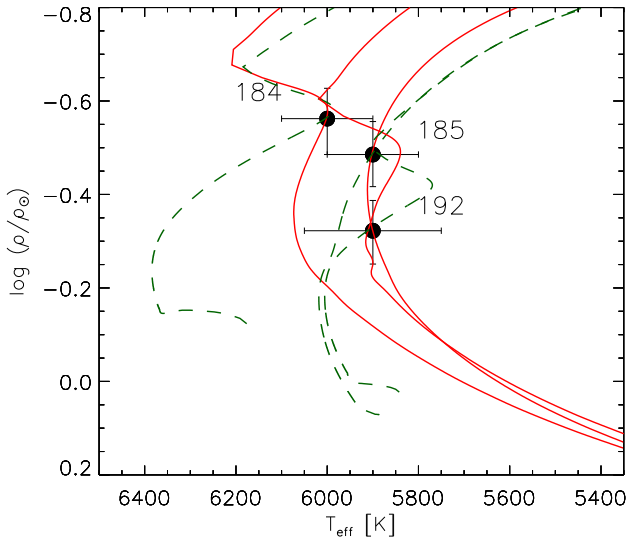

Figure 1. The host star's effective temperature ($T_{\rm eff}$) versus density, each symbol being labelled by the WASP planet number). We show best-fit evolution tracks (green dashed lines) and isochrones (red solid lines) for the masses, ages and [Fe/H] values listed in Table 2.

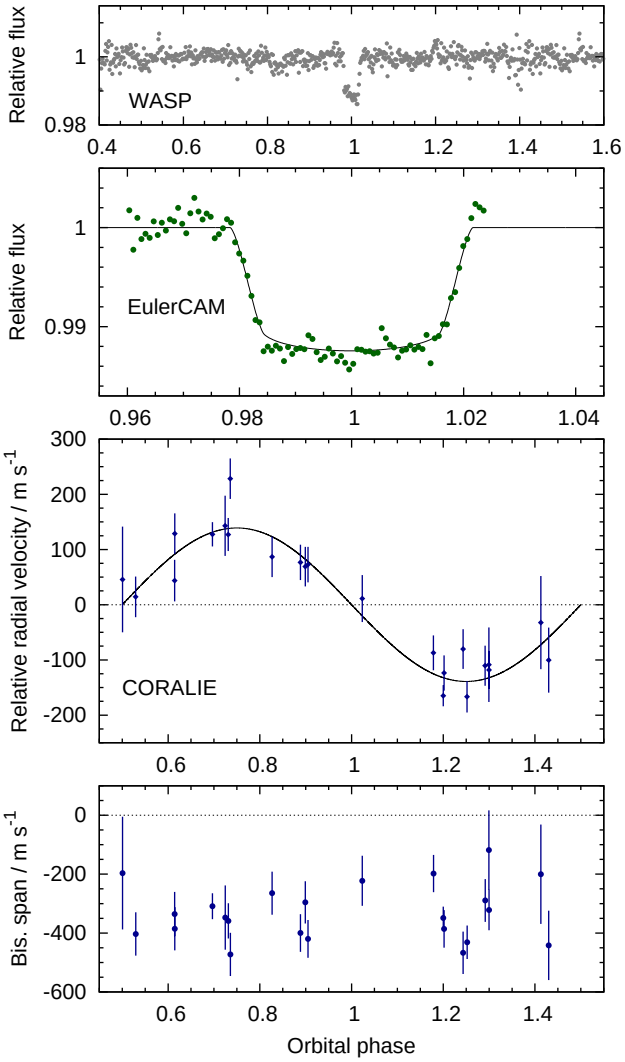

Figure 2. WASP-178b discovery data: (Top) The WASP data folded on the transit period. (Second panel) The EulerCAM transit lightcurve together with the fitted MCMC model. (Third panel) The CORALIE RV data and fitted model. (Bottom) The bisector spans of the CORALIE data.

tion of a hot-Jupiter orbit is often shorter than the time in its current orbit). To fit the transit photometry we adopted limb-darkening coefficients by interpolating from the 4-parameter, non-linear law of Claret (2000), as appropriate for the star's temperature and metallicity. The WASP passband and the TRAPPIST "blue block" filter are wide, non-standard pass bands, for which we approximate by using R-band coefficients, which is sufficient for the quality of our photometry. The MCMC code includes a step where the error bars are inflated such that the fit to each dataset has a χ^2_ν of 1. This allows for red noise not accounted for in the input errors, thus balancing the different datasets and increasing the output error ranges. An account of the effects of red noise in typical WASP-planet discovery datasets is given in Smith et al. (2012).

The parameters resulting from the MCMC analysis are listed in the tables for each system. $T_{\rm c}$ is the mid-transit epoch, P is the orbital period, ΔF is the transit depth that would be observed in the absence of limb-darkening, T_{14} is the duration from first to fourth contact, b the impact parameter, and K_1 the stellar reflex velocity. For WASP-184, WASP-185 and WASP-192 the BAGEMASS outputs are tabulated in Table 2 while the best-fit stellar evolution tracks and isochrones are shown in Fig. 1 (WASP-178 is too hot for the BAGEMASS code to be reliable).

5 WASP-178

WASP-178 (= HD 134004) is a bright, V = 9.95, star for which the spectral analysis suggests $T_{\rm eff}$ = 9350 ± 150 K and an A1 IV–V classification (Table 3; Fig. 2). It appears to be a mild hot Am star, slightly enhanced in Fe ([Fe/H] = +0.21 ± 0.16) and slightly depleted in Ca and Sc ([Ca/H] = –0.06 ± 0.14; [Sc/H] = –0.35 ± 0.08). Y and Ba are also enhanced by +0.35 ± 0.10 and +0.96 ± 0.15, respectively. Interstellar Na D lines lead to an estimate of $E(B–V)$ = 0.06 ± 0.01, which then implies (through the Infra Red Flux Method) a $T_{\rm eff}$ of 9390 ± 190 K, consistent with that from the spectral analysis. The projected rotation speed is relatively low at $v \sin i$ = 8.2 ± 0.6 km s^{-1} (measured assuming zero macro-turbulence). We report (Table 3) a stellar mass of 2.07 ± 0.11 M$_\odot$ and a stellar radius of 1.67 ± 0.07 R$_\odot$, which are compatible with a main-sequence, non-evolved status.

WASP-178 appears to be relatively isolated on the sky, with no nearby stars within 17 arcsec listed in GAIA DR2, and all stars within 30 arcsecs being >7 magnitudes fainter. However, WASP-178 is noted in GAIA DR2 as having significant excess noise in the astrometry, amounting to 0.18 mas in 254 astrometric observations. This could indicate an unresolved and unseen binary companion.

With a temperature of 9350 ± 150 K, WASP-178 is

Table 2. Bayesian mass and age estimates for the host stars using GARSTEC stellar models assuming $\alpha_{\rm MLT} = 1.78$. Columns 2, 3 and 4 give the maximum-likelihood estimates of the age, mass, and initial metallicity, respectively. Columns 5 and 6 give the mean and standard deviation of their posterior distributions. The systematic errors on the mass and age due to uncertainties in the mixing length and helium abundance are given in Columns 7 to 10.

Star	$\tau_{\rm iso,b}$ [Gyr]	$M_{\rm b}[M_\odot]$	$[{\rm Fe/H}]_{\rm i,b}$	$\langle\tau_{\rm iso}\rangle$ [Gyr]	$\langle M_\star\rangle$ $[M_\odot]$	$\sigma_{\tau,Y}$	$\sigma_{\tau,\alpha}$	$\sigma_{M,Y}$	$\sigma_{M,\alpha}$
WASP-184	4.0	1.29	+0.168	4.66 ± 1.15	1.245 ± 0.072	−0.13	0.40	−0.036	−0.005
WASP-185	7.2	1.09	+0.066	6.63 ± 1.58	1.116 ± 0.068	0.23	1.87	−0.048	−0.069
WASP-192	5.1	1.16	+0.215	5.70 ± 1.92	1.137 ± 0.069	0.21	0.98	−0.043	−0.016

Table 3. System parameters for WASP-178.

1SWASP J150904.89-424217.7
HD 134004; 2MASS 15090488–4242178
GAIA RA = $15^{\rm h}09^{\rm m}04.89^{\rm s}$, Dec = $-42^\circ42'17.8''$ (J2000)
V mag = 9.95; GAIA G = 9.91; J = 9.77
Rotational modulation: < 1.5 mmag
GAIA DR2 pm (RA) –10.01 ± 0.12 (Dec) –5.65 ± 0.10 mas/yr
GAIA DR2 parallax: 2.3119 ± 0.0600 mas
Distance = 418 ± 16 pc

Stellar parameters from spectroscopic analysis.	
Spectral type	A1 IV–V
$T_{\rm eff}$ (K)	9350 ± 150
$\log g$	4.35 ± 0.15
$v \sin i$ (km s^{-1})	8.2 ± 0.6
Microturbulence (km s^{-1})	2.9 ± 0.2
[Fe/H]	+0.21 ± 0.16
[Ca/H]	–0.06 ± 0.14
[Sc/H]	–0.35 ± 0.08
[Cr/H]	+0.43 ± 0.10
[Y/H]	+0.35 ± 0.10
[Ba/H]	+0.96 ± 0.15
[Ni/H]	+0.32 ± 0.12
Parameters from MCMC analysis.	
P (d)	3.3448285 ± 0.0000012
$T_{\rm c}$ (HJD) (UTC)	245 6927.06839 ± 0.00047
T_{14} (d)	0.1446 ± 0.0016
$T_{12} = T_{34}$ (d)	0.0197 ± 0.0016
$\Delta F = R_{\rm P}^2/{\rm R}_*^2$	0.01243 ± 0.00028
b	0.54 ± 0.05
i (°)	85.7 ± 0.6
K_1 (km s^{-1})	0.139 ± 0.009
γ (km s^{-1})	−23.908 ± 0.007
e	0 (adopted) (< 0.08 at 2σ)
a/R_*	7.17 ± 0.21
M_* ($M_\odot$)	2.07 ± 0.11
R_* ($R_\odot$)	1.67 ± 0.07
$\log g_*$ (cgs)	4.31 ± 0.04
ρ_* ($\rho_\odot$)	0.44 ± 0.05
$T_{\rm eff}$ (K)	9360 ± 150
$M_{\rm P}$ ($M_{\rm Jup}$)	1.66 ± 0.12
$R_{\rm P}$ ($R_{\rm Jup}$)	1.81 ± 0.09
$\log g_{\rm P}$ (cgs)	3.07 ± 0.05
$\rho_{\rm P}$ ($\rho_{\rm J}$)	0.28 ± 0.05
a (AU)	0.0558 ± 0.0010
$T_{\rm P,A=0}$ (K)	2470 ± 60

Priors were $M_* = 2.04 \pm 0.12$ $M_\odot$ and $R_* = 1.81 \pm 0.12$ $R_\odot$
Errors are 1σ; Limb-darkening coefficients were:
R band: a1 = 0.669, a2 = –0.223, a3 = 0.280, a4 = –0.125
I band: a1 = 0.724, a2 = –0.616, a3 = 0.644, a4 = –0.245

the second hottest known host of a hot Jupiter, behind the A0 star KELT-9 (Gaudi et al. 2017) at 10 170 K and ahead of the A2 star MASCARA-2/KELT-20 (Lund et al. 2017; Talens et al. 2018) at 8980 K.

Despite the high stellar temperature, CORALIE RVs are able to detect the orbital motion. The planet is in a 3.3-day orbit with a mass of 1.66 ± 0.12 $M_{\rm Jup}$ and a bloated radius of 1.81 ± 0.09 $R_{\rm Jup}$. The estimated equilibrium temperature is 2470 ± 60 K, the hottest of any planet with an orbital period of > 3 d. Fig. 2 shows the transit photometry and radial-velocity orbit. We also plot the bisector spans against phase, where the absence of a correlation is a check against transit mimics (e.g. Queloz et al. 2001).

6 WASP-184

WASP-184 is a V = 12.9, G0 star with a metallicity of [Fe/H] = +0.12 ± 0.08 and a distance of 640 ± 28 pc (Table 4; Fig. 3). WASP-184 is relatively isolated with no stars recorded in GAIA DR2 within 10 arcsecs, and only 2 stars (>6 magnitudes fainter) within 30 arcsecs. There is no excess astrometric noise recorded in DR2. The mass and radius of WASP-184 (1.23 ± 0.07 $M_\odot$; 1.65 ± 0.09 $R_\odot$) imply that it is evolving off the main sequence. Using the BAGEMASS code we compute an age of 4.7 ± 1.1 Gyr. Lithium depletion to the measured value of log A(Li)= 2.04 ± 0.08 could take ∼5 Gyr according to Table 3 of Sestito & Randich (2005), which is consistent with the BAGEMASS age.

The system is reasonably well parametrised by a partial transit from TRAPPIST-South, a nearly-full transit from EulerCAM, and 19 RVs from CORALIE. The planet is in a 5.18-d orbit and is a moderately bloated, lower-mass hot Jupiter (0.57 ± 0.07 $M_{\rm Jup}$; 1.33 ± 0.09 $R_{\rm Jup}$).

7 WASP-185

WASP-185 is a V = 11.1, G0 star with a solar metallicity ([Fe/H] = –0.02 ± 0.06) at a distance of 275 ± 6 pc (Table 5; Fig. 4). It has an apparent companion star 4.6 arcsecs away and 4.4 mag fainter in GAIA G (too faint for GAIA to report its proper motion, so we don't know whether the two are physically associated; at the distance of WASP-185 the separation would correspond to 1200 AU). Otherwise WASP-185 is relatively isolated (with 3 other stars, >9 magnitudes fainter, between 20 and 30 arcsecs away). There is no DR2 excess astrometric noise reported for WASP-185. The companion star is sufficiently distant that it will not affect the CORALIE RVs, however it is included in the extraction

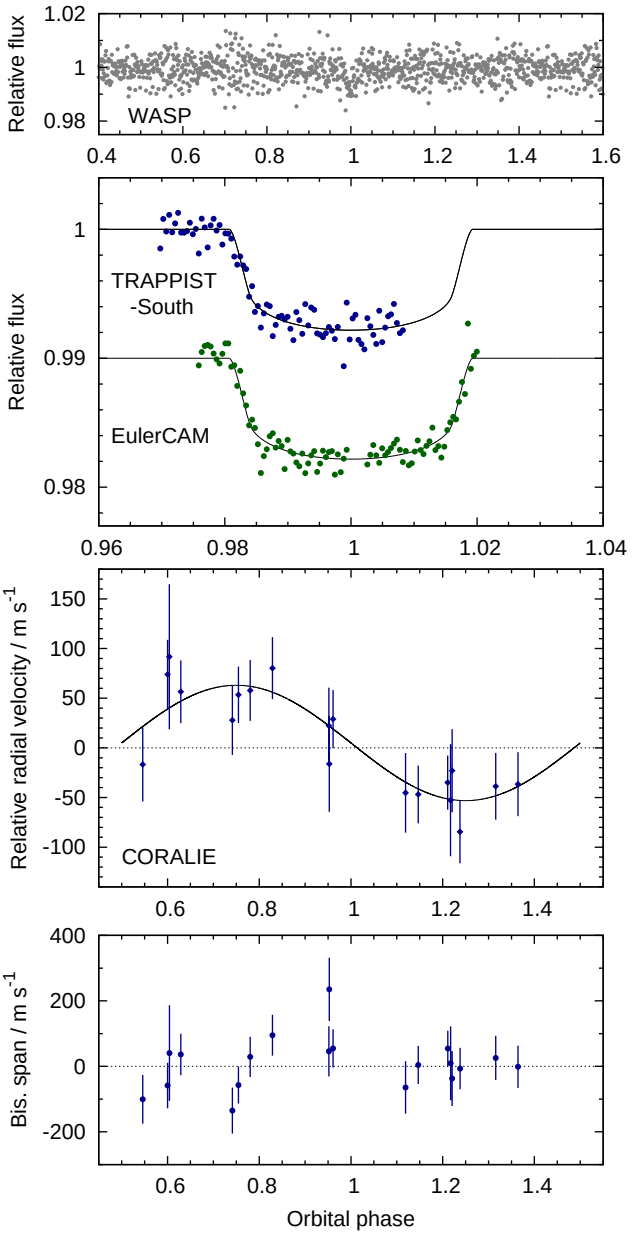

Figure 3. WASP-184b discovery data and fitted model, as for Fig. 2. The TRAPPIST, EulerCAM and CORALIE observations are listed in Table 1.

Table 4. System parameters for WASP-184.

1SWASP J135804.10–302053.0	
2MASS 13580408–3020532	
GAIA RA = $13^{h}58^{m}04.09^{s}$, Dec = $-30°20'53.3''$ (J2000)	
V mag = 12.9; GAIA G = 12.57; J = 11.6	
Rotational modulation: < 2 mmag	
GAIA DR2 pm (RA) –4.36 ± 0.06 (Dec) –5.09 ± 0.06 mas/yr	
GAIA DR2 parallax: 1.480 ± 0.037 mas	
Distance = 640 ± 28 pc	
Stellar parameters from spectroscopic analysis.	
Spectral type	G0
$T_{\rm eff}$ (K)	6000 ± 100
$\log g$	4.0 ± 0.2
$v \sin i$ (km s^{-1})	4.5 ± 1.1
[Fe/H]	+0.12 ± 0.08
log A(Li)	2.04 ± 0.08
Parameters from MCMC analysis.	
P (d)	5.18170 ± 0.00001
$T_{\rm c}$ (HJD) (UTC)	245 7630.008 ± 0.001
T_{14} (d)	0.1990 ± 0.0027
$T_{12} = T_{34}$ (d)	0.0187 ± 0.0024
$\Delta F = R_{\rm P}^2/R_*^2$	0.0069 ± 0.0003
b	0.44 ± 0.14
i (°)	86.9 ± 1.1
K_1 (km s^{-1})	0.058 ± 0.010
γ (km s^{-1})	8.366 ± 0.008
e	0 (adopted) (< 0.25 at 2σ)
a/R_*	8.19 ± 0.42
M_* ($M_\odot$)	1.23 ± 0.07
R_* ($R_\odot$)	1.65 ± 0.09
$\log g_*$ (cgs)	4.09 ± 0.05
ρ_* ($\rho_\odot$)	0.27 ± 0.05
$T_{\rm eff}$ (K)	6000 ± 100
$M_{\rm P}$ ($M_{\rm Jup}$)	0.57 ± 0.10
$R_{\rm P}$ ($R_{\rm Jup}$)	1.33 ± 0.09
$\log g_{\rm P}$ (cgs)	2.87 ± 0.10
$\rho_{\rm P}$ ($\rho_{\rm J}$)	0.24 ± 0.07
a (AU)	0.0627 ± 0.0012
$T_{\rm P,A=0}$ (K)	1480 ± 50
Priors were M_* = 1.25 ± 0.07 $M_\odot$ and R_* = 1.59 ± 0.10 $R_\odot$	
Errors are 1σ; Limb-darkening coefficients were:	
R band: a1 = 0.578, a2 = 0.022, a3 = 0.359, a4 = –0.230	

aperture for the TRAPPIST photometry. We therefore applied a correction of 1.8% to the transit photometry, though in practice this amount is much less than the uncertainties.

The mass and radius of WASP-185 (1.12 ± 0.06 $M_\odot$; 1.50 ± 0.08 $R_\odot$) indicate an evolved star, and the BAGEMASS code suggests an age of 6.6 ± 1.6 Gyr. Lithium depletion to the measured value of log A(Li) = 2.37 ± 0.09 could take ∼2 Gyr, but this abundance of lithium is found in NGC 188 which is ∼8 Gyr old according to Table 3 of Sestito & Randich (2005). Thus the lithium is consistent with the BAGEMASS age.

We have only limited photometry of the transit, one ingress and one egress, both obtained in deteriorating observing conditions, and so the transit parameterisation depends substantially on the stellar radius deduced from the GAIA DR2 distance. Our 24 CORALIE RVs trace out an eccentric orbit, though there is clearly additional scatter of unknown origin. This could be magnetic activity of the host star, though no rotational modulation is seen in the WASP data to a limit of 1 mmag (WASP-166 is an example of a system showing RV variation owing to magnetic activity, but no rotational modulation; Hellier et al. 2019b).

The planet's orbit has a relatively long period for a hot Jupiter, at 9.39 d, and has an eccentricity of e = 0.24 ± 0.04. The impact factor is relatively high at b = 0.81 ± 0.03. The planet's mass and radius (0.98 ± 0.06 $M_{\rm Jup}$; 1.25 ± 0.08 $R_{\rm Jup}$) are typical for hot Jupiters.

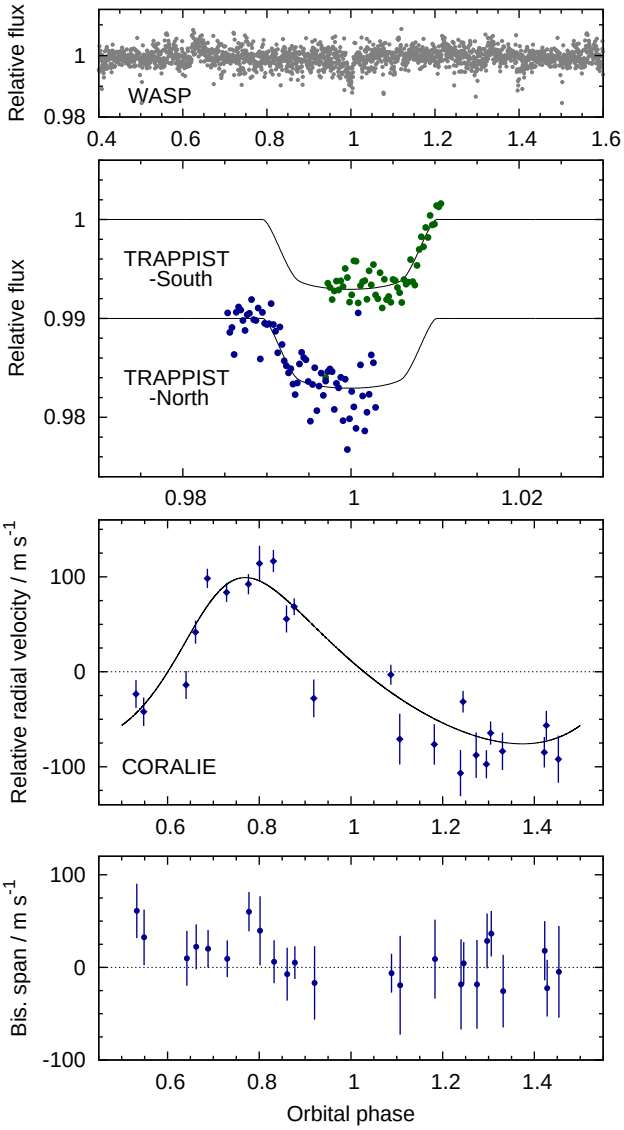

Figure 4. WASP-185b discovery data and fitted model, as for Figs. 2 & 3.

Table 5. System parameters for WASP-185.

1SWASP J141614.30–193232.1	
2MASS 14161431–1932321	
GAIA RA = $14^h16^m14.31^s$, Dec = $-19°32'32.2''$ (J2000)	
V mag = 11.1; GAIA G = 10.89; J = 9.87	
Rotational modulation: < 1 mmag	
GAIA DR2 pm (RA) –13.40 ± 0.08 (Dec) –6.06 ± 0.07 mas/yr	
GAIA DR2 parallax: 3.552 ± 0.043 mas	
Distance = 275 ± 6 pc	
Stellar parameters from spectroscopic analysis.	
Spectral type	G0
$T_{\rm eff}$ (K)	5900 ± 100
$\log g$	4.0 ± 0.2
$v \sin i$ (km s^{-1})	2.8 ± 0.9
[Fe/H]	–0.02 ± 0.06
log A(Li)	2.37 ± 0.09
Parameters from MCMC analysis.	
P (d)	9.38755 ± 0.00002
$T_{\rm c}$ (HJD) (UTC)	245 6935.982 ± 0.002
T_{14} (d)	0.192 ± 0.006
$T_{12} = T_{34}$ (d)	0.040 ± 0.006
$\Delta F = R_{\rm P}^2/R_*^2$	0.0073 ± 0.0005
b	0.81 ± 0.03
i (°)	86.8 ± 0.3
K_1 (km s^{-1})	0.088 ± 0.004
γ (km s^{-1})	23.874 ± 0.003
e	0.24 ± 0.04
ω (deg)	–42 ± 7
a/R_*	12.9 ± 0.7
M_* ($M_\odot$)	1.12 ± 0.06
R_* ($R_\odot$)	1.50 ± 0.08
$\log g_*$ (cgs)	4.13 ± 0.05
ρ_* ($\rho_\odot$)	0.33 ± 0.06
$T_{\rm eff}$ (K)	5900 ± 100
$M_{\rm P}$ ($M_{\rm Jup}$)	0.98 ± 0.06
$R_{\rm P}$ ($R_{\rm Jup}$)	1.25 ± 0.08
$\log g_{\rm P}$ (cgs)	3.15 ± 0.07
$\rho_{\rm P}$ ($\rho_{\rm J}$)	0.50 ± 0.12
a (AU)	0.0904 ± 0.0017
$T_{\rm P,A=0}$ (K)	1160 ± 35
Priors were M_* = 1.11 ± 0.06 $M_\odot$ and R_* = 1.58 ± 0.09 $R_\odot$	
Errors are 1σ; Limb-darkening coefficients were:	
R band: a1 = 0.568, a2 = –0.009, a3 = 0.443, a4 = –0.271	
z band: a1 = 0.651, a2 = –0.334, a3 = 0.621, a4 = –0.320	

8 WASP-192

WASP-192 is a V = 12.3, G0 star with metallicity [Fe/H] = +0.14 ± 0.08 at a distance of 495 ± 22 pc (Table 6; Fig. 5). It is isolated in the sky, with no stars, less than 6 magnitudes fainter, within 30 arcsecs according to GAIA DR2. There is no excess astrometric noise reported in DR2. The mass and radius (1.09 ± 0.06 $M_\odot$; 1.32 ± 0.07 $R_\odot$) indicate a moderately evolved star, and the BAGEMASS code produces an age of 5.7 ± 1.9 Gyr. Lithium depletion to the measured log A(Li) = 2.11 ± 0.13 could take ∼5 Gyr according to Table 3 of Sestito & Randich (2005), which is consistent with the BAGEMASS age.

The planet WASP-192b has a typical hot-Jupiter orbit of P = 2.88 d with a relatively high impact parameter of b = 0.84 ± 0.03. We have TRAPPIST photometry of one partial transit and one full transit, though that was in poorer observing conditions. The planet is more massive than average for a hot Jupiter at 2.30 ± 0.16 $M_{\rm Jup}$, such that 12 CORALIE RVs show a well-defined orbital motion. The radius of 1.23 ± 0.08 $R_{\rm Jup}$ is typical of hot Jupiters that have masses in the range 2–3 $M_{\rm Jup}$.

9 DISCUSSION

Recent papers have outlined a class of "ultra-hot Jupiters", defined by Parmentier et al. (2018) as Jupiters with day-side temperatures greater than 2200 K. Atmospheric characterisation of UHJs such as WASP-18b, WASP-103b and WASP-121b (e.g. Kreidberg et al. 2018a; Arcangeli et al. 2019) has revealed systematically different behaviour from cooler planets. Whereas cooler planets can show strong water features (e.g. WASP-107b; Kreidberg et al. 2018b) water is thought

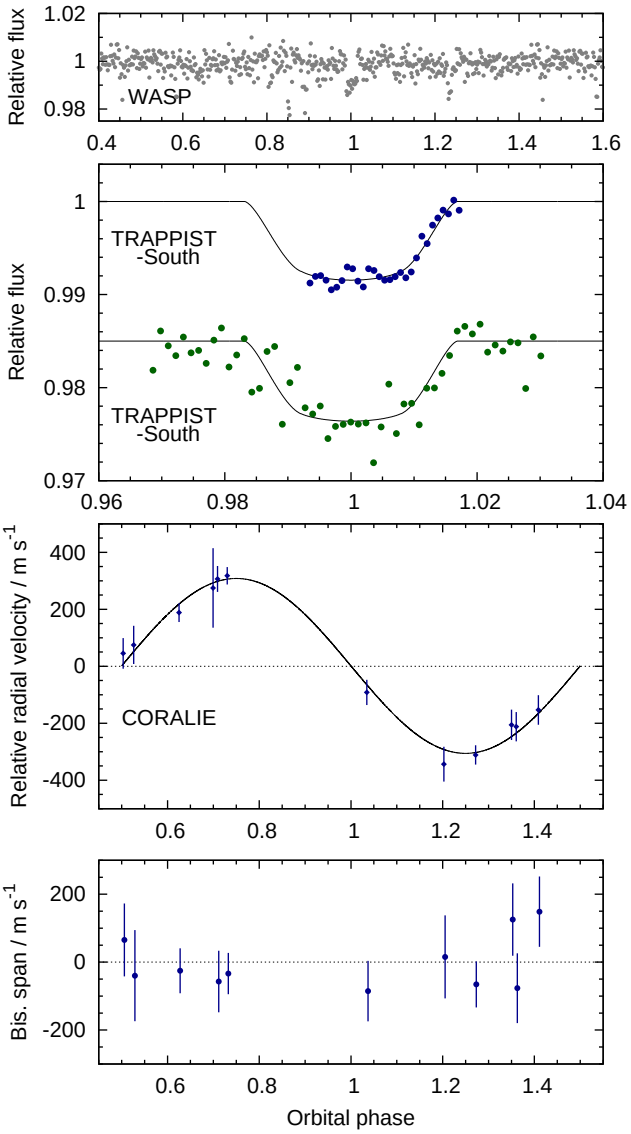

Figure 5. WASP-192b discovery data and fitted model, as for Figs. 2 & 3.

Table 6. System parameters for WASP-192.

1SWASP J145438.06–384439.6	
2MASS 14543809–3844403	
GAIA RA = $14^{\rm h}54^{\rm m}38.09^{\rm s}$, Dec = $-38^\circ44'40.3''$ (J2000)	
V mag = 12.3; GAIA G = 12.53; J = 11.5	
Rotational modulation: < 2 mmag	
GAIA DR2 pm (RA) 0.72 ± 0.07 (Dec) –1.53 ± 0.06 mas/yr	
GAIA DR2 parallax: 1.939 ± 0.062 mas	
Distance = 495 ± 22 pc	
Stellar parameters from spectroscopic analysis.	
Spectral type	G0
$T_{\rm eff}$ (K)	5900 ± 150
$\log g$	4.5 ± 0.2
$v \sin i$ (km s^{-1})	3.1 ± 1.1
[Fe/H]	+0.14 ± 0.08
log A(Li)	2.11 ± 0.13
Parameters from MCMC analysis.	
P (d)	2.8786765 ± 0.0000028
$T_{\rm c}$ (HJD) (UTC)	245 7271.3331 ± 0.0017
T_{14} (d)	0.0964 ± 0.0040
$T_{12} = T_{34}$ (d)	0.026 ± 0.004
$\Delta F = R_{\rm P}^2/{\rm R}_*^2$	0.00926 ± 0.00061
b	0.84 ± 0.03
i (°)	82.7 ± 0.6
K_1 (km s^{-1})	0.307 ± 0.017
γ (km s^{-1})	15.896 ± 0.013
e	0 (adopted) (< 0.25 at 2σ)
a/R_*	6.65 ± 0.34
M_* ($M_\odot$)	1.09 ± 0.06
R_* ($R_\odot$)	1.32 ± 0.07
$\log g_*$ (cgs)	4.236 ± 0.051
ρ_* ($\rho_\odot$)	0.476 ± 0.080
$T_{\rm eff}$ (K)	5910 ± 145
$M_{\rm P}$ ($M_{\rm Jup}$)	2.30 ± 0.16
$R_{\rm P}$ ($R_{\rm Jup}$)	1.23 ± 0.08
$\log g_{\rm P}$ (cgs)	3.54 ± 0.07
$\rho_{\rm P}$ ($\rho_{\rm J}$)	1.22 ± 0.31
a (AU)	0.0408 ± 0.0008
$T_{\rm P,A=0}$ (K)	1620 ± 60
Priors were M_* = 1.09 ± 0.06 $M_\odot$ and R_* = 1.34 ± 0.08 $R_\odot$	
Errors are 1σ; Limb-darkening coefficients were:	
R band: a1 = 0.621, a2 = –0.179, a3 = 0.655, a4 = –0.356	
I band: a1 = 0.697, a2 = –0.435, a3 = 0.801, a4 = –0.394	

to disassociate on the day-sides of UHJs, such that no water features are seen. The disassociated ions then drift to the night side, where they recombine. The molecule CO, however, has a stronger molecular bond, and is still present on the day sides of UHJs, where it can produce an emission feature (e.g. Parmentier et al. 2018).

In Table 7 we list the hottest of all the known UHJs, those with a calculated equilibrium temperature above 2300 K (the UHJ definition of *day-side* temperature > 2200 K includes many more objects than we list). We use equilibrium temperature, taking the data from TEPcat[2] WASP-178b now joins this group. Transiting a V = 9.95 star, it is among the best UHJ targets visible from the Southern Hemisphere, along with WASP-18b, WASP-103b, WASP-121b and WASP-189b.

A correlation between high irradiation of hot Jupiters and bloated radii is now well established (e.g. Hartman et al. 2016; Bhatti et al. 2016; Sestovic et al. 2018). WASP-178b is at the upper end of such a relationship, as illustrated for known planets in Fig. 6. Also apparent in Table 7 is a tendency for the hottest HJs to be more massive than typical. The median mass of a transiting hot Jupiter is ∼0.9 $M_{\rm Jup}$, whereas the median of those in Table 7 is 2.2 $M_{\rm Jup}$. This presumably reflects the destruction of irradiated gas giants by photo-evaporation (e.g. Owen & Lai 2018), such that lower-mass UHJs would have short lifetimes. Indeed, lower-mass UHJs such as WASP-12b (1.5 $M_{\rm Jup}$) are seen to be losing mass (e.g. Fossati et al. 2013). With a moderate mass of 1.7 $M_{\rm Jup}$, WASP-178b is thus also a candidate for photo-evaporation.

[2] https://www.astro.keele.ac.uk/jkt/tepcat/ (Southworth 2011), since it can be calculated uniformly for all the known systems.

Table 7. The hottest of all known ultra-hot Jupiters

Name	Eq. Temp (K)	Host	Host V	Period (d)	Radius (Jup)	Mass (Jup)	Discovery
KELT-9b	4050	A0	7.6	1.48	1.89	2.9	Gaudi et al. (2017)
WASP-33b	2780	A5	8.3	1.22	1.60	2.1	Collier Cameron et al. (2010)
Kepler-13b	2750	A2	10.0	1.76	1.41	∼9	Shporer et al. (2011)
WASP-189b	2640	A6	6.6	2.72	1.40	1.9	Anderson et al. (2018)
WASP-12b	2590	G0	11.7	1.09	1.90	1.5	Hebb et al. (2009)
MASCARA-1b	2570	A8	8.3	2.15	1.50	3.7	Talens et al. (2017)
HAT-P-70b	2560		9.5	2.74	1.87		Zhou et al. (2019)
WASP-103b	2510	F8	12.0	0.92	1.53	1.5	Gillon et al. (2014)
WASP-178b	2470	A1	9.9	3.34	1.81	1.7	This work
WASP-78b	2470	F8	12.0	2.17	2.06	0.9	Smalley et al. (2012)
KELT-16b	2450	F7	11.9	0.97	1.42	2.7	Oberst et al. (2017)
WASP-18b	2410	F9	9.3	0.94	1.20	10.5	Hellier et al. (2009)
WASP-121b	2360	F6	10.4	1.27	1.87	1.2	Delrez et al. (2016)
WASP-167b/KELT-13b	2330	F1	10.5	2.02	1.51		Temple et al. (2017)
WASP-87Ab	2320	F5	10.7	1.68	1.39	2.2	Anderson et al. (2014)

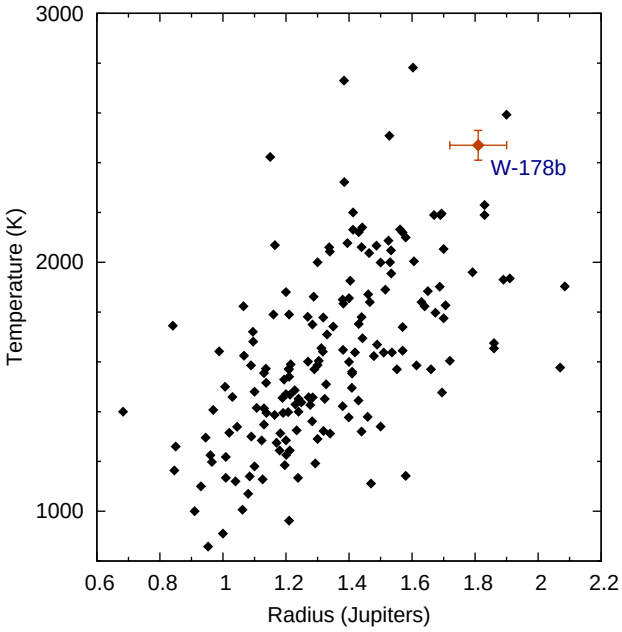

Figure 6. Radii and calculated temperatures of transiting hot Jupiters, showing the location of WASP-178b in red. KELT-9b is above the plot at 4600 K. The data are from http://exoplanet.eu. We caution about selection effects in such a plot since non-bloated planets would have shallower transits against larger, hotter stars, so would be harder to detect.

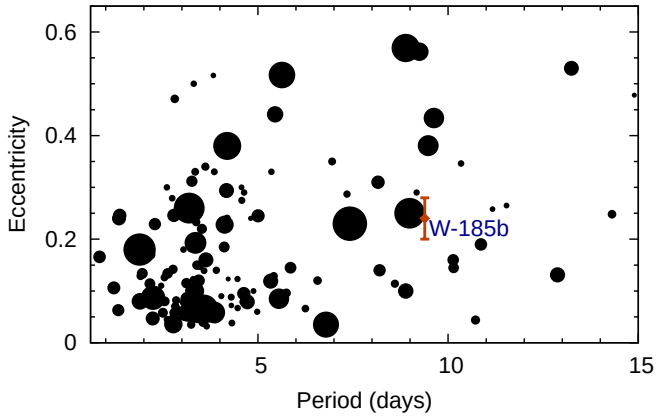

Figure 7. Orbital eccentricity versus orbital period for hot Jupiters, with WASP-185b's location in red. Only systems with $e > 0.03$ are shown. The symbol area scales with the planet mass. Data are from http://exoplanet.eu.

We turn now to WASP-185b, which is notable for its eccentric orbit of $e = 0.24$. The tidal circularisation timescale increases markedly with orbital period, and so eccentric orbits are more likely for longer periods such as WASP-185b's 9.39 d (see Fig. 7). Using eqn 3 of Adams & Laughlin (2006) we can estimate the circularisation timescale of WASP-185b as $\sim$2 Gyr, though this depends on assuming $Q_P \sim 10^5$, which is uncertain. There is a tendency, however, for hot Jupiters with eccentric orbits to be either more massive (e.g. WASP-8b at 2.2 M_{Jup}; Queloz et al. 2010, WASP-162b at 5.2 M_{Jup}; Hellier et al. 2019a, and HAT-P-34b at 3.3 M_{Jup}; Bakos et al. 2012) or to have indications of additional bodies in the system that might be perturbing the hot Jupiter (e.g. HAT-P-31b,c; Kipping et al. 2011 and HAT-P-17b,c; Howard et al. 2012). Given that WASP-185b is only 1 M_{Jup}, and so should circularise more rapidly, and given the relatively long 6.6 ± 1.6 Gyr age of the host star, it may be that WASP-185b has arrived in its current orbit more recently, or that it is being perturbed by an outer companion (e.g. Petrovich & Tremaine 2016), possibly the putative companion at 1200 AU. It would thus be worthwhile to obtain Rossiter–McLaughlin observations of WASP-185b to discern whether the planet's orbit is aligned or mis-aligned with the stellar rotation.

ACKNOWLEDGEMENTS

WASP-South was hosted by the South African Astronomical Observatory and we are grateful for their support and assistance. Funding for WASP came from consortium universities and from the UK's Science and Technology Facilities Council. The Euler Swiss telescope is supported by the Swiss Na-

tional Science Foundation. The research leading to these results has received funding from the ARC grant for Concerted Research Actions, financed by the Wallonia-Brussels Federation. TRAPPIST-South is funded by the Belgian Fund for Scientific Research (Fond National de la Recherche Scientifique, FNRS) under the grant FRFC 2.5.594.09.F, with the participation of the Swiss National Science Fundation (SNF). MG and EJ are F.R.S.-FNRS Senior Research Associates.

REFERENCES

Adams F. C., Laughlin G., 2006, ApJ, 649, 1004
Anderson D. R., et al., 2012, MNRAS, 422, 1988
Anderson D. R., et al., 2014, arXiv e-prints, p. arXiv:1410.3449
Anderson D. R., et al., 2018, arXiv e-prints, p. arXiv:1809.04897
Arcangeli J., et al., 2019, A&A, 625, A136
Bakos G. Á., et al., 2012, AJ, 144, 19
Barkaoui K., et al., 2019, AJ, 157, 43
Bhatti W., et al., 2016, arXiv e-prints, p. arXiv:1607.00322
Blackwell D. E., Shallis M. J., 1977, MNRAS, 180, 177
Boyajian T. S., et al., 2013, ApJ, 771, 40
Claret A., 2000, A&A, 363, 1081
Collier Cameron A., et al., 2007a, MNRAS, 375, 951
Collier Cameron A., et al., 2007b, MNRAS, 380, 1230
Collier Cameron A., et al., 2010, MNRAS, 407, 507
Delrez L., et al., 2016, MNRAS, 458, 4025
Doyle A. P., et al., 2013, MNRAS, 428, 3164
Doyle A. P., Davies G. R., Smalley B., Chaplin W. J., Elsworth Y., 2014, MNRAS, 444, 3592
Fossati L., Ayres T. R., Haswell C. A., Bohlender D., Kochukhov O., Flöer L., 2013, ApJ, 766, L20
Gaia Collaboration et al., 2016, A&A, 595, A1
Gaia Collaboration et al., 2018, A&A, 616, A1
Gaudi B. S., et al., 2017, Nature, 546, 514
Gillon M., et al., 2013, A&A, 552, A82
Gillon M., et al., 2014, A&A, 562, L3
Hartman J. D., et al., 2016, AJ, 152, 182
Hebb L., et al., 2009, ApJ, 693, 1920
Hellier C., et al., 2009, Nature, 460, 1098
Hellier C., et al., 2019a, MNRAS, 482, 1379
Hellier C., et al., 2019b, MNRAS, 488, 3067
Howard A. W., et al., 2012, ApJ, 749, 134
Kipping D. M., et al., 2011, AJ, 142, 95
Kreidberg L., et al., 2018a, AJ, 156, 17
Kreidberg L., Line M. R., Thorngren D., Morley C. V., Stevenson K. B., 2018b, ApJ, 858, L6
Lendl M., et al., 2012, A&A, 544, A72
Lund M. B., et al., 2017, AJ, 154, 194
Maxted P. F. L., et al., 2011, PASP, 123, 547
Maxted P. F. L., Serenelli A. M., Southworth J., 2015, A&A, 575, A36
Niemczura E., Smalley B., Pych W., 2014, Determination of Atmospheric Parameters of B-, A-, F- and G-Type Stars, doi:10.1007/978-3-319-06956-2.
Oberst T. E., et al., 2017, AJ, 153, 97
Owen J. E., Lai D., 2018, MNRAS, 479, 5012
Parmentier V., et al., 2018, A&A, 617, A110
Pepe F., Mayor M., Galland F., Naef D., Queloz D., Santos N. C., Udry S., Burnet M., 2002, A&A, 388, 632
Petrovich C., Tremaine S., 2016, ApJ, 829, 132
Pollacco D. L., et al., 2006, PASP, 118, 1407
Queloz D., et al., 2001, A&A, 379, 279
Queloz D., et al., 2010, A&A, 517, L1
Ricker G. R., et al., 2016, in Space Telescopes and Instrumentation 2016: Optical, Infrared, and Millimeter Wave. p. 99042B, doi:10.1117/12.2232071
Sestito P., Randich S., 2005, A&A, 442, 615
Sestovic M., Demory B.-O., Queloz D., 2018, A&A, 616, A76
Shporer A., et al., 2011, AJ, 142, 195
Smalley B., et al., 2012, A&A, 547, A61
Smith A. M. S., et al., 2012, AJ, 143, 81
Southworth J., 2011, MNRAS, 417, 2166
Stassun K. G., Torres G., 2018, ApJ, 862, 61
Talens G. J. J., et al., 2017, A&A, 606, A73
Talens G. J. J., et al., 2018, A&A, 612, A57
Temple L. Y., et al., 2017, MNRAS, 471, 2743
Triaud A. H. M. J., et al., 2013, A&A, 551, A80
Weiss A., Schlattl H., 2008, Ap&SS, 316, 99
Zhou G., et al., 2019, arXiv e-prints, p. arXiv:1906.00462

Table A1. Radial velocities.

BJD − 2400 000 (UTC)	RV (km s^{-1})	σ_{RV} (km s^{-1})	Bisector (km s^{-1})
WASP-178:			
57850.91018	−24.0725	0.0192	−0.3486
57893.80235	−23.8966	0.0426	−0.2225
57894.56659	−24.0744	0.0285	−0.4313
57904.73294	−24.0182	0.0364	−0.2893
57934.67540	−23.9881	0.0360	−0.4670
57949.66427	−23.7647	0.0545	−0.3473
57951.58735	−24.0164	0.0675	−0.1183
57952.64066	−23.8640	0.0377	−0.3355
57954.60536	−24.0314	0.0319	−0.3859
57955.60534	−23.8620	0.0957	−0.1964
57958.65602	−23.9400	0.0843	−0.2004
57959.60533	−23.7802	0.0220	−0.3087
57974.59726	−23.9948	0.0316	−0.1979
58002.52881	−23.8935	0.0367	−0.4032
58018.48523	−24.0258	0.0345	−0.3217
58020.49026	−23.8387	0.0359	−0.2958
58030.48938	−23.8311	0.0320	−0.3998
58203.89388	−23.7806	0.0299	−0.3586
58207.82049	−23.8350	0.0322	−0.4199
58247.69603	−23.8210	0.0366	−0.2646
58276.47209	−24.0082	0.0590	−0.4419
58277.49486	−23.6794	0.0367	−0.4725
58320.57235	−23.7790	0.0367	−0.3855
WASP-184:			
57190.68828	8.3083	0.0564	0.0095
57618.50533	8.4188	0.0306	0.0288
57817.78113	8.2765	0.0317	−0.0066
57905.73109	8.3261	0.0273	0.0545
57924.47781	8.4413	0.0312	0.0950
57933.67645	8.4528	0.0730	0.0404
57954.53219	8.4176	0.0317	0.0363
57959.56409	8.4350	0.0347	−0.0586
58170.79185	8.3245	0.0323	−0.0012
58171.73350	8.3443	0.0372	−0.1005
58172.74625	8.3889	0.0350	−0.1351
58173.88416	8.3900	0.0292	0.0547
58174.70319	8.3157	0.0400	−0.0645
58175.72199	8.3224	0.0337	0.0258
58247.77332	8.3381	0.0419	−0.0371
58277.47072	8.3834	0.0384	0.0459
58307.53963	8.4145	0.0284	−0.0570
58308.56619	8.3448	0.0482	0.2351
58309.57037	8.3142	0.0291	0.0041
58593.66628	8.0600	0.0625	0.0982

Bisector errors are twice RV errors

BJD − 2400 000 (UTC)	RV (km s^{-1})	σ_{RV} (km s^{-1})	Bisector (km s^{-1})
WASP-185:			
57191.68952	23.7717	0.0243	−0.0183
57193.69299	23.7864	0.0248	−0.0048
57194.58975	23.8364	0.0150	0.0324
57218.60712	23.8076	0.0267	−0.0193
57221.56637	23.7937	0.0160	0.0179
57412.87431	23.9926	0.0187	0.0396
57487.74786	23.9708	0.0106	0.0601
57488.68674	23.9470	0.0089	0.0051
57591.52359	23.9950	0.0116	0.0061
57599.55951	23.9768	0.0102	0.0201
57809.83999	23.8754	0.0105	−0.0063
57815.86446	23.9621	0.0099	0.0093
57820.70709	23.8470	0.0114	0.0043
57901.58066	23.9342	0.0143	−0.0072
57905.75841	23.8140	0.0123	0.0364
57918.49287	23.9202	0.0122	0.0222
57933.62653	23.7907	0.0239	−0.0183
57951.54401	23.8020	0.0213	0.0090
57952.60960	23.7811	0.0148	0.0286
57990.48949	23.7948	0.0196	−0.0256
58311.55039	23.8551	0.0147	0.0610
58312.57675	23.8646	0.0148	0.0097
58324.57747	23.8505	0.0198	−0.0167
58357.50144	23.8219	0.0153	−0.0224
WASP-192:			
57568.61900	15.5839	0.0340	−0.0655
58312.63770	16.2129	0.0304	−0.0336
58329.60684	16.0837	0.0331	−0.0253
58541.83740	15.6896	0.0533	0.1255
58542.87037	16.2018	0.0453	−0.0570
58543.80761	15.8034	0.0445	−0.0852
58544.74536	15.6832	0.0514	−0.0766
58544.88449	15.7419	0.0518	0.1486
58545.72117	16.1702	0.1396	0.2143
58576.82272	15.9405	0.0537	0.0655
58576.88842	15.9702	0.0671	−0.0397
58578.83595	15.5516	0.0611	0.0154

Bisector errors are twice RV errors